

Behavior and Sensitivity of Phase Arrival Times (PHASE)

Emmanuel Skarsoulis

Foundation for Research and Technology Hellas
Institute of Applied and Computational Mathematics
100 N. Plastira str., GR-70013 Heraklion, Greece
phone: +30-2810-391776 fax: +30-2810-391801
email: eskars@iacm.forth.gr

in collaboration with

Bruce Cornuelle and Matthew Dzieciuch
Scripps Institution of Oceanography
University of California, San Diego
La Jolla, CA 92093-0225
phone: (858) 534-4021 fax: (858) 534-9820
email: bdc@ucsd.edu, mad@ucsd.edu

Award Number: N00014-13-1-0366
<http://www.iacm.forth.gr>, <http://sio.ucsd.edu>

LONG-TERM GOALS

Our long-term goal is to study the sensitivity behavior of acoustic phase arrival times, as an alternative observable offering increased resolution (compared to peak arrivals), for the recovery of sound-speed perturbations in the ocean.

OBJECTIVES

The objective of this work is to study the behavior and sensitivity of ocean acoustic phase arrival times due to sound-speed changes, in comparison to those of peak arrival times. The aim is to derive perturbation relations and sensitivity kernels connecting sound-speed and travel-time perturbations, and, further, to study the behavior of phase arrival times and its predictability, depending on propagation and signal characteristics.

APPROACH

Phase arrival times are mathematically modeled as stationary points - times of constant phase - of the acoustic pressure. Using this definition, expressions for the corresponding travel-time perturbations are derived and the sensitivity behavior of phase arrival times, due to sound speed changes, is studied. The resulting sensitivity kernels (Born-Frechet kernels) for phase arrival times are compared to the corresponding travel-time sensitivity kernels for peak arrivals.

Report Documentation Page				Form Approved OMB No. 0704-0188	
Public reporting burden for the collection of information is estimated to average 1 hour per response, including the time for reviewing instructions, searching existing data sources, gathering and maintaining the data needed, and completing and reviewing the collection of information. Send comments regarding this burden estimate or any other aspect of this collection of information, including suggestions for reducing this burden, to Washington Headquarters Services, Directorate for Information Operations and Reports, 1215 Jefferson Davis Highway, Suite 1204, Arlington VA 22202-4302. Respondents should be aware that notwithstanding any other provision of law, no person shall be subject to a penalty for failing to comply with a collection of information if it does not display a currently valid OMB control number.					
1. REPORT DATE 30 SEP 2014		2. REPORT TYPE		3. DATES COVERED 00-00-2014 to 00-00-2014	
4. TITLE AND SUBTITLE Behavior and Sensitivity of Phase Arrival Times (PHASE)				5a. CONTRACT NUMBER	
				5b. GRANT NUMBER	
				5c. PROGRAM ELEMENT NUMBER	
6. AUTHOR(S)				5d. PROJECT NUMBER	
				5e. TASK NUMBER	
				5f. WORK UNIT NUMBER	
7. PERFORMING ORGANIZATION NAME(S) AND ADDRESS(ES) University of California San Diego, Scripps Institution of Oceanography, 9500 Gilman Drive, La Jolla, CA, 92093				8. PERFORMING ORGANIZATION REPORT NUMBER	
9. SPONSORING/MONITORING AGENCY NAME(S) AND ADDRESS(ES)				10. SPONSOR/MONITOR'S ACRONYM(S)	
				11. SPONSOR/MONITOR'S REPORT NUMBER(S)	
12. DISTRIBUTION/AVAILABILITY STATEMENT Approved for public release; distribution unlimited					
13. SUPPLEMENTARY NOTES					
14. ABSTRACT					
15. SUBJECT TERMS					
16. SECURITY CLASSIFICATION OF:			17. LIMITATION OF ABSTRACT Same as Report (SAR)	18. NUMBER OF PAGES 10	19a. NAME OF RESPONSIBLE PERSON
a. REPORT unclassified	b. ABSTRACT unclassified	c. THIS PAGE unclassified			

RESULTS

Mathematical modeling and perturbation expressions

The complex pressure at the receiver in the time domain [1] can be written in the form

$$p(t) = a(t)e^{i\varphi(t)}e^{i\omega_0 t}, \quad (1)$$

where t denotes time, $a(t)$ is the amplitude (arrival pattern), $\varphi(t)$ is the phase and ω_0 is the central (carrier) circular frequency of the source. The demodulated pressure results after removal of the carrier frequency and can alternatively be expressed in terms of its real and imaginary parts, $u(t)$ and $v(t)$:

$$\tilde{p}(t) = a(t)e^{i\varphi(t)} = u(t) + iv(t) \quad (2)$$

The above quantities $a(t)$, $\varphi(t)$, $u(t)$, and $v(t)$ depend on the source/receiver location as well as on the sound-speed distribution $c(\mathbf{x})$, where \mathbf{x} is the spatial variable. Thus, perturbations $\delta c(\mathbf{x})$ of the sound speed give rise to perturbations in arrival amplitude, arrival phase and arrival times. Peak arrival times are defined as the times of the local maxima (peak arrivals) of the arrival pattern: $\dot{a}(\tau_p; c) = 0$. As the sound speed changes the peaks of the arrival pattern are deformed and displaced, i.e. peak arrival times change as well. The resulting perturbation relation reads [1]

$$\delta\tau_p = -\frac{\delta\dot{a}_1(\tau_p; c; \delta c)}{\ddot{a}(\tau_p; c)} = -\frac{\dot{u}\delta u_1 + u\delta\dot{u}_1 + \dot{v}\delta v_1 + v\delta\dot{v}_1}{\dot{u}^2 + u\ddot{u} + \dot{v}^2 + v\ddot{v}}, \quad (3)$$

where the quantities u , v and their time derivatives are considered at the background state (c) and their 1st-order perturbations are due to δc .

Phase arrival times are defined as fixed-level crossings of the phase [3]

$$\psi(t) = \varphi(t) + \omega_0 t \quad (4)$$

Due to the term $\omega_0 t$, the phase $\psi(t)$ is rapidly increasing with time. Phase arrival times τ_ψ are defined as $\psi(\tau_\psi) = \gamma$, where γ is a fixed threshold (e.g. $\gamma = 2n\pi$ corresponds to maxima, $\gamma = \pi/2 + 2n\pi$ to zero crossings of the real part of $p(t)$). By applying the definition at the background and perturbed state and using a Taylor expansion of the latter we obtain

$$\delta\tau_\psi = -\frac{\delta\varphi}{\dot{\varphi} + \omega_0} = -\frac{u\delta v - v\delta u}{u\dot{v} - v\dot{u} + \omega_0(u^2 + v^2)} \quad (5)$$

By comparing eqs. (3) and (5) we see that the perturbation expressions for peak and phase arrival are different, so the two time observables will behave differently, in general. This is quite anticipated since the two observables correspond to different functions, peak arrival times to the amplitude function $a(t)$ and phase arrival times to the phase function $\psi(t)$.

Sensitivity kernels of phase arrival times

The complex pressure p at the receiver in the time domain, and its perturbation δp due to perturbations of the sound speed distribution, can be expressed through the inverse Fourier transform in terms of the signal $P_s(\omega)$ emitted by the source in the frequency domain and the frequency-domain Green's function $G_{sr}(\omega; c; \mathbf{x}_r | \mathbf{x}_s)$ and its perturbation $\delta G_{sr}(\omega; c; \delta c; \mathbf{x}_r | \mathbf{x}_s)$, respectively

$$p(t) = \frac{1}{2\pi} \int_{-\infty}^{+\infty} P_s(\omega) G(\omega; c; \mathbf{x}_r | \mathbf{x}_s) e^{i\omega t} d\omega \quad \text{and} \quad \delta p(t) = \frac{1}{2\pi} \int_{-\infty}^{+\infty} P_s(\omega) \delta G(\omega; c; \delta c; \mathbf{x}_r | \mathbf{x}_s) e^{i\omega t} d\omega \quad (6)$$

where \mathbf{x}_s and \mathbf{x}_r is the source and receiver position vector. The perturbation of the Green's function can be expressed through the first Born approximation [1], which in 3-dimensional space reads

$$\delta G_{3D}(\omega; c; \delta c; \mathbf{x}_r | \mathbf{x}_s) = -2\omega^2 \iiint_V G_{3D}(\omega; c; \mathbf{x} | \mathbf{x}_s) G_{3D}(\omega; c; \mathbf{x}_r | \mathbf{x}) \frac{\delta c(\mathbf{x})}{c^3(\mathbf{x})} dV(\mathbf{x}). \quad (7)$$

Assuming a range-independent background environment the 3-dimensional Green's function can be written in terms of normal modes [2]

$$G_{3D}(r, z | z_s) = \frac{e^{-i\pi/4}}{\rho_w \sqrt{8\pi}} \sum_{m=1}^M \frac{\varphi_m(z_s) \varphi_m(z)}{\sqrt{k_m r}} e^{-ik_m r}, \quad (8)$$

where ρ_w is the water density and k_m and $\varphi_m(z)$ are the real eigenvalues and the corresponding eigenfunctions of the vertical Sturm-Liouville problem. By substituting eq. (8) into eq. (7) and using the perturbation relations, eqs. (3) and (5), expressions of the form

$$\delta\tau = \iiint_V K_\tau^{(3D)}(\mathbf{x}) \delta c(\mathbf{x}) dV(\mathbf{x}) \quad (9)$$

can be obtained, where $K_\tau^{(3D)}(\mathbf{x})$ is the corresponding 3-dimensional travel-time sensitivity kernel, describing the effect that a sound-speed perturbation at location \mathbf{x} will have on the travel time τ of interest. In two dimensions the Green's function reads [2]

$$G_{2D}(x, z | z_s) = \frac{e^{-i\pi/2}}{2\rho_w} \sum_{m=1}^M \frac{\varphi_m(z_s) \varphi_m(z)}{k_m} e^{-ik_m x}, \quad (10)$$

and its perturbations are given by the 2D Born approximation

$$\delta G_{2D}(\omega; c; \delta c; \mathbf{x}_r | \mathbf{x}_s) = -2\omega^2 \iint_A G_{2D}(\omega; c; \mathbf{x} | \mathbf{x}_s) G_{2D}(\omega; c; \mathbf{x}_r | \mathbf{x}) \frac{\delta c(\mathbf{x})}{c^3(\mathbf{x})} dA(\mathbf{x}). \quad (11)$$

where the integral is now a 2D integral over the 2D perturbation area A . These equations result in the following integral perturbation expression between travel time perturbations and underlying sound-speed perturbations

$$\delta\tau = \int_A K_\tau^{(2D)}(\mathbf{x}) \delta c(\mathbf{x}) dA(\mathbf{x}) \quad (12)$$

where $K_{\tau}^{(2D)}(\mathbf{x})$ is the corresponding 2-dimensional travel-time sensitivity kernel.

Shallow-water environment

Some numerical results for travel-time sensitivity kernels of peak and phase arrival times in a shallow-water environment are presented in the following. Results for deep-water environments were included in previous reports [3]. A Pekeris shallow-water waveguide, shown in Fig. 1, is considered. The water depth is 200 m and the sound speed in the water is taken 1500 m/s. The bottom is taken to be a half space of sound speed 1900 m/sec. Source and receiver are at a depth of 50 m – marked by the dots in Fig. 1 – and horizontal distance of 3 km. The acoustic signal is a Gaussian pulse with central frequency 300 Hz and bandwidth 70 Hz (3-dB bandwidth).

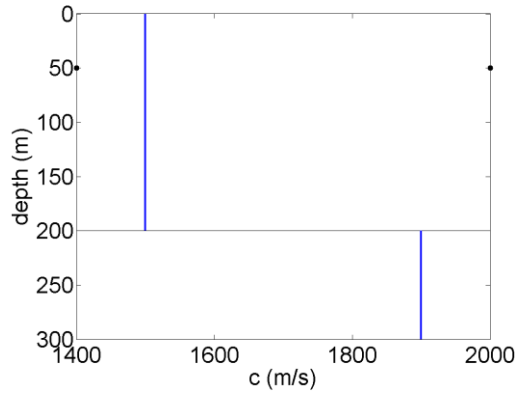


Fig. 1. Pekeris waveguide

Fig. 2 shows at the top the 2D arrival pattern on the left and the acoustic pressure at the receiver in the time domain (real part) on the right. The lower panels show the 2D travel-time sensitivity kernels corresponding to the 3 marked peaks (peak arrival times on the left and phase arrival times on the right). The arrival pattern in this case, opposite to deep-water propagation, starts with near-horizontal arrivals corresponding to low-order modes and continues with gradually steeper arrivals, with increasing separation, until the critical angle is reached. The real part of the received pressure on the right shows a modulated version of the arrival pattern with modulation frequency corresponding to the central source frequency, 300 Hz. The 3 marked phase arrivals on the top right are selected to be closest – in time – to the selected 3 peak arrivals on the top left.

The sensitivity kernel of the first peak arrival (peak 1) represents the superposition of two propagation paths, one surface-reflected and one bottom-reflected, interfering in the time domain. The underlying arrivals and corresponding propagation paths can be resolved by increasing the bandwidth (see Fig. 5 below). The sensitivity kernel of the first phase arrival corresponds to the surface reflected path. The arrival corresponding to the direct (horizontal) path cannot be resolved / separated from the surface-reflected arrival, because the difference between the corresponding path lengths is very small (1.7 m) resulting in a difference in arrival times of 1.1 msec. The kernels of the later arrivals correspond to steeper acoustic paths with larger number of surface and bottom reflections. Peak and phase travel-time sensitivity kernels for those arrivals are comparable in shape and magnitude.

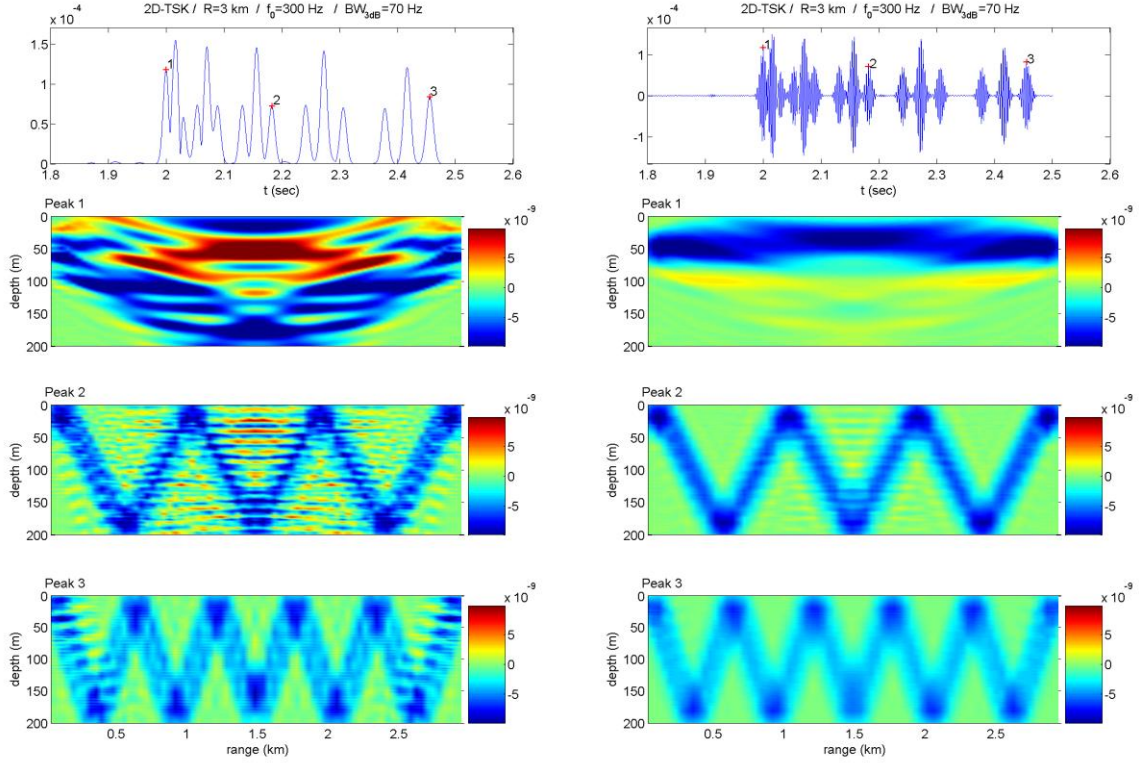


Fig. 2. 2D propagation results in the Pekeris waveguide at 3 km range. Left: Arrival pattern and sensitivity kernels for peak arrival times of marked peaks. Right: Acoustic pressure and sensitivity kernels for phase arrival times of marked peaks.

Fig. 3 shows the 3D propagation results for the arrival pattern and peak arrival time sensitivity kernels – vertical section through the source and receiver – on the left and the received acoustic pressure and phase arrival time sensitivity kernels on the right. While the arrival pattern and acoustic pressure are very similar to the 2D results of Fig. 2 the 3D sensitivity kernels of the peak and phase arrivals exhibit a large difference in magnitude, with the peak arrival time sensitivity being much weaker than the sensitivity of phase arrival times. This difference points to a dissimilar off-plane behavior of the 3D kernels for the phase and peak arrivals.

Fig. 4 shows the vertical cross-section (cross-range direction) of the 3D peak and phase arrival time sensitivity kernels at 1.5 km range, i.e. in the middle between source and receiver. From the right-hand panels of this figure it is seen that the sensitivity of phase arrival times exhibits near-axial symmetry about its core along with a strong alternating behavior, which causes cancelation of the central high sensitivity values when horizontal cross-range marginals are taken. On the other hand the negative 3D sensitivity of the peak arrival times (left) extends in the horizontal cross-range direction and this causes an amplification of the central values. This indicates that the two observables sample changes in the water mass differently, phase arrival times within the Fresnel zone about the eigenrays and peak arrival times in the horizontal cross-range direction, sideways from the eigenray.

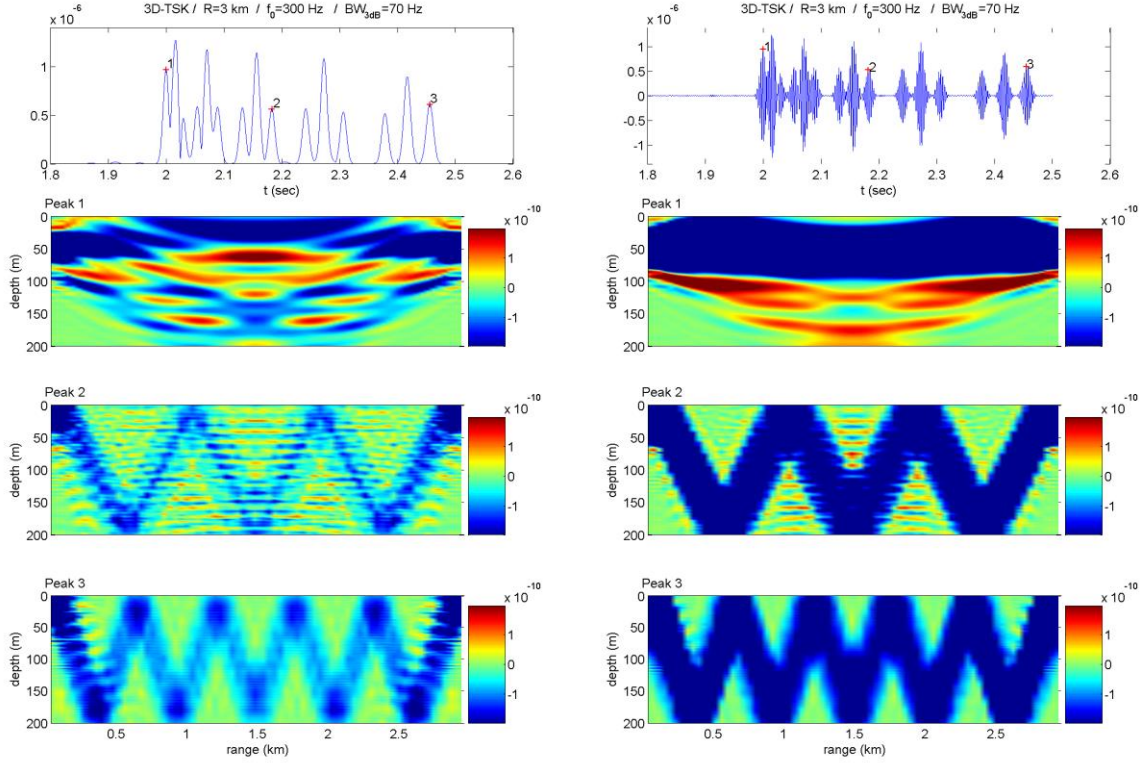


Fig. 3. 3D propagation results in the Pekeris waveguide at 3 km range. Left: Arrival pattern and sensitivity kernels on the vertical source-receiver plane for peak arrival times of marked peaks. Right: Acoustic pressure and sensitivity kernels for phase arrival times of marked peaks.

Fig. 5 shows higher-resolution propagation results and sensitivity kernels resulting from a triple-fold increase in the signal bandwidth (210 Hz). This leads to a corresponding decrease in the pulse duration such that overlapping arrivals can be resolved as can be seen in the case of the congested early arrivals (near-horizontal propagation paths). In that case the first peak in Fig. 2 is the superposition of the first two peak arrivals in Fig. 5, and its sensitivity kernel splits into two sensitivity kernels one corresponding to the surface-reflected and one to the bottom-reflected path, peaks 1 and 2 in Fig. 5, respectively. Note that the time difference between these two arrivals is 10 msec and can be resolved with the 210-Hz bandwidth (5-msec pulse duration), but not with a 70-Hz bandwidth (14-msec pulse duration). The third peak arrival in Fig. 5 is a double arrival corresponding to two symmetric propagation paths, with one surface and one bottom reflection each. Coming to the sensitivities of the phase arrival times, the situation is similar as for the peak arrivals. The interesting point in the case of phase arrivals is that in order to resolve the two different propagation paths, the surface- and the bottom-reflected one, it is not necessary to increase the bandwidth. Fig. 6 shows at the top a detailed view of the early part of the 70-Hz arrival pattern shown in Fig. 2 and 3 phase arrivals selected, with times close to those of the selected three arrivals in Fig. 5. The sensitivity kernels shown underneath are practically the same as the ones obtained with a triple-fold bandwidth in Fig. 5. This is a significant advantage of phase arrivals and the corresponding travel time sensitivity kernels.

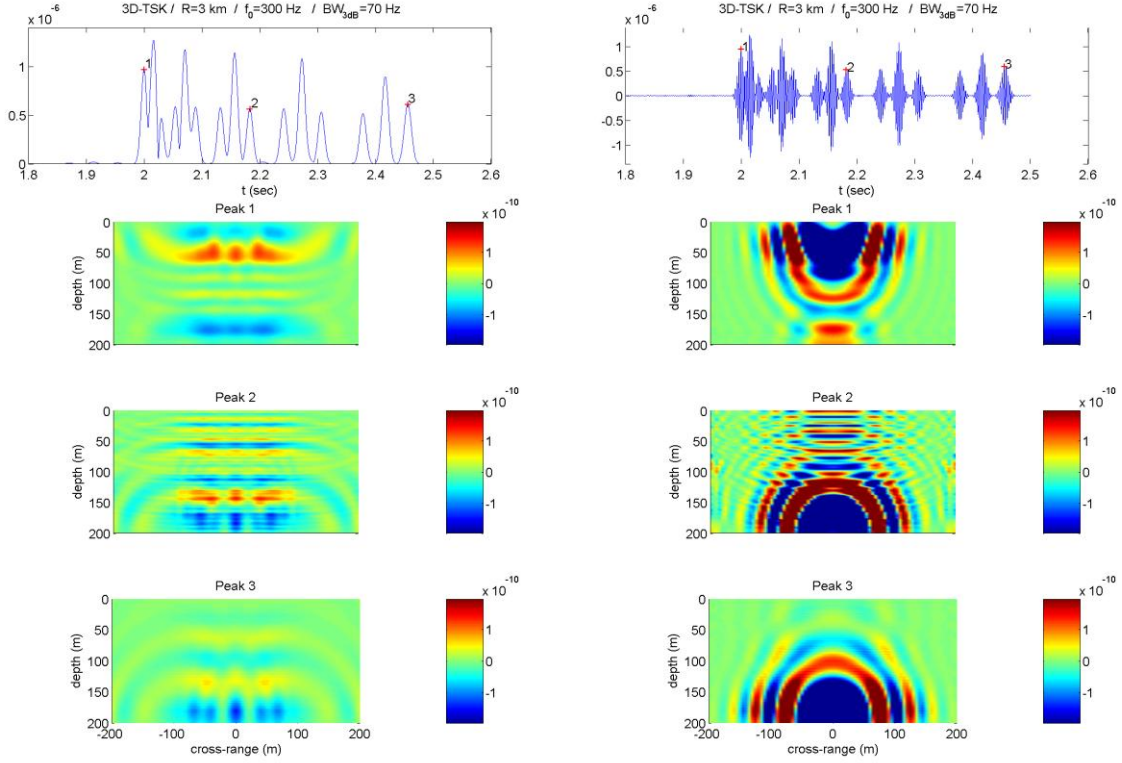


Fig. 4. 3D propagation results in the Pekeris waveguide at 3 km range. Left: Arrival pattern and sensitivity kernel cross-sections at mid range for peak arrival times of marked peaks. Right: Acoustic pressure and sensitivity kernel cross-sections for phase arrival times of marked peaks

In the following the vertical sensitivity kernels of peak and phase arrivals for the Pekeris waveguide are considered. In Fig. 7 a schematic diagram of an eigenray connecting source and receiver is shown. Assuming source and receiver at the same depth and horizontal distance R , and also assuming constant sound speed c in the water, the travel time from the source to the receiver along the direct (horizontal) acoustic path is $\tau = c / R$ (2 sec for the Pekeris environment considered). The travel-time perturbation for a sound speed change δc is $\delta \tau = -\delta c R / c^2$. Thus, the travel-time sensitivity distributed over the water depth h and normalized by the propagation range R becomes $\delta \tau / \delta c / (Rh) = -1 / hc^2$. For the considered Pekeris environment/geometry ($h=200$ m, $c=1500$ m/sec) this equals $-2.22 \text{ sec}^2/\text{km}^2$.

The steepest propagating path is that corresponding to the critical angle φ_{CR} , which for the considered Pekeris environment/geometry ($c=1500$ m/sec in the water and 1900 m/sec in the bottom) equals 37.9° . The length R' of the corresponding acoustic path is $R' = R / \cos(\varphi_{CR})$ and the travel time is $\tau' = c / R'$ and $\delta \tau' = -\delta c R' / c^2$. Thus the travel-time sensitivity distributed over the water depth h and normalized by the propagation range R becomes $\delta \tau' / \delta c / (Rh) = -R' / Rhc^2 = -1 / hc^2 \cos(\varphi_{CR})$. For the considered Pekeris environment/geometry ($h=200$ m, $c=1500$ m/sec, $\varphi_{CR} = 37.9^\circ$) this equals $-2.8 \text{ sec}^2/\text{km}^2$. Thus the ray-theoretic vertical travel-time sensitivity kernel takes value between -2.22 (early arrivals) and $-2.8 \text{ sec}^2/\text{km}^2$ (late arrivals).

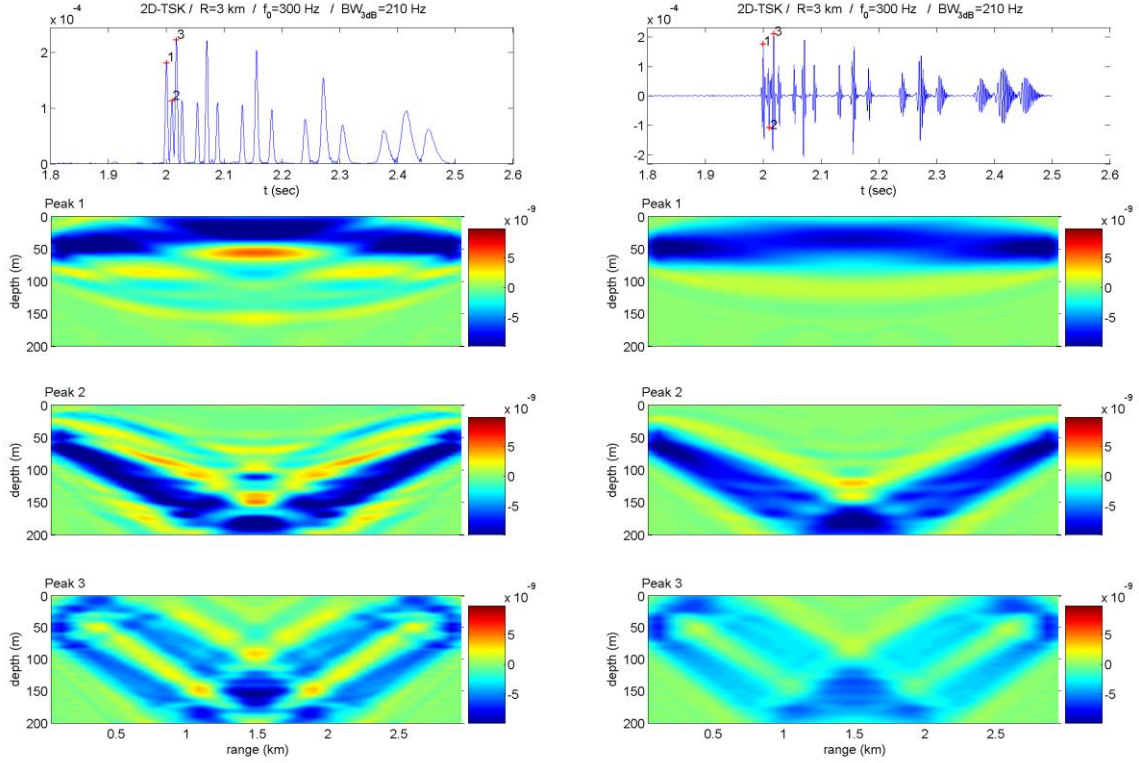


Fig. 5. 2D propagation results in the Pekeris waveguide using a bandwidth of 210 Hz. Left: Arrival pattern and peak arrival time sensitivity kernels for 3 marked peaks. Right: Received acoustic pressure and phase arrival time sensitivity kernels for 3 marked peaks.

Fig. 8 shows the wave-theoretic vertical travel-time sensitivity kernels for the 3 peak arrival times (left) and for the 3 phase arrival times (right) selected in Fig. 2. The above mentioned ray-theoretic limiting values are also shown in Fig. 8 as dashed lines. A first remark from Fig. 8 is that the vertical sensitivity kernels for peak arrival times exhibit a much more oscillatory behavior than those for phase arrival times. Apart from that, the sensitivity kernels are uniform with respect to depth, as far as the intermediate and late arrivals are concerned. The sensitivity of the first arrival on the other hand exhibits large deviations from its average value both for the peak and the phase arrival time. The average values of all 3 peaks lie within the ray-theoretic limits (dashed lines). Further, the sensitivity magnitude grows stronger for later arrivals, in agreement with the ray-theoretic behavior. Finally, the sensitivity of phase arrivals appears to be slightly weaker than that of peak arrivals which points to different perturbation behavior of phase and peak arrivals, in general, due to sound speed perturbations.

IMPACT/APPLICATIONS

The phase arrival times offer higher temporal resolution than peak arrivals, since their width is controlled by the central source frequency rather than the source bandwidth. Furthermore, while peak arrivals require broadband (low-Q) sources, phase arrivals can be resolved even in the case of smaller bandwidths, which means cheaper sources. The sensitivity and perturbation behavior of phase arrivals is in general different from that of peak arrivals, and large deviations may occur between the

perturbations of the two observables, depending on the location (the spatial support) of the underlying sound-speed change. Phase arrival times exhibit good predictability in the studied cases, i.e. the first-order predictions based on the sensitivity kernels lie close to the actual time perturbations. Thus, phase arrival times offer a useful alternative to peak arrivals as observables for ocean acoustic tomography. The exploitation of peak arrival times requires dense sampling in time, in order to keep track of the phase (2π -ambiguity) as the ocean (sound speed) changes.

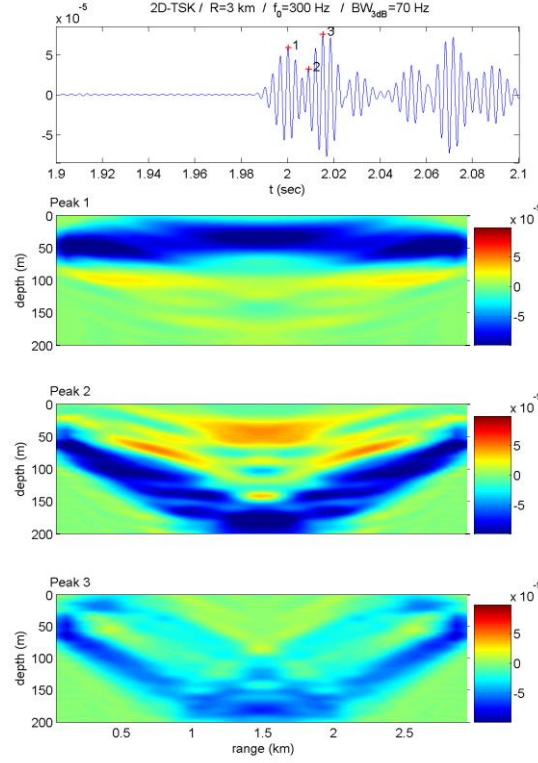


Fig. 6. Received acoustic pressure (detail) and phase arrival time sensitivity kernels for 3 early phase arrivals (marked) in the Pekeris waveguide using a bandwidth of 70 Hz.

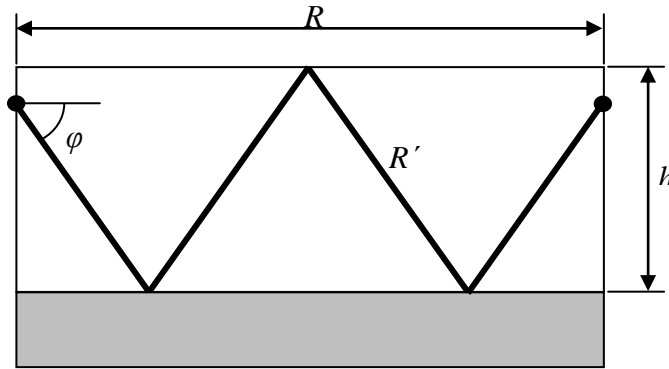


Fig. 7. Schematic eigenray diagram for Pekeris waveguide

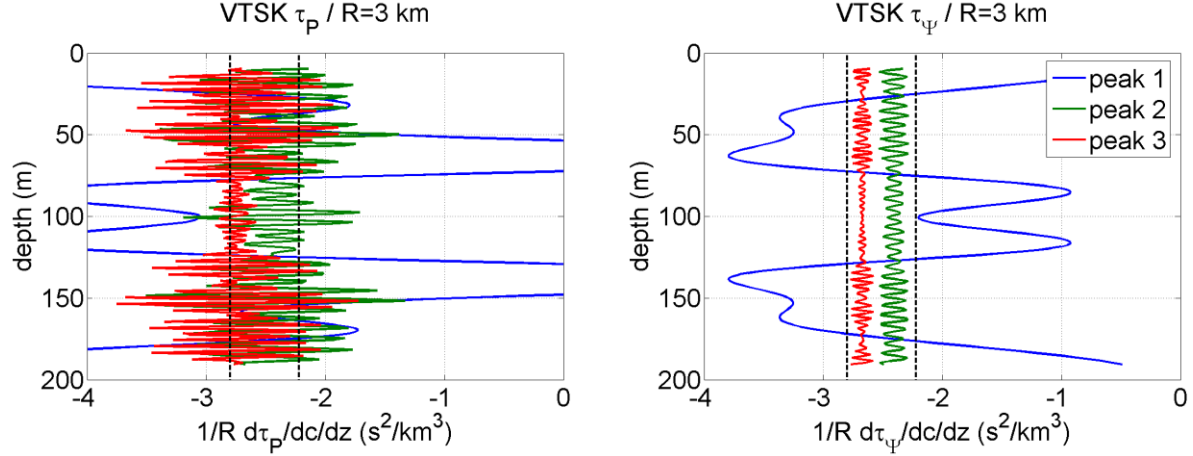


Fig. 8: Normalized vertical sensitivity kernels in the Pekeris waveguide for peak arrival times (left) and phase arrival times (right) of the 3 peaks marked in Fig. 2. The vertical dashed lines mark the limiting values corresponding to horizontal and critical-angle propagation, respectively.

REFERENCES

- [1] E.K. Skarsoulis, B.D. Cornuelle, ‘Travel-time sensitivity kernels in ocean acoustic tomography’, *J. Acoust. Soc. Am.* 116, pp. 227-238, 2004.
- [2] E.K. Skarsoulis, B.D. Cornuelle, M.A. Dzieciuch, Travel-time sensitivity kernels in long-range propagation, *Journal of the Acoustical Society of America*, Vol. 126, pp. 2223-2233, 2009

PUBLICATIONS

- [3] E.K. Skarsoulis, B.D. Cornuelle, M.A. Dzieciuch, Sensitivity behavior of phase and peak arrival times, in Proc. 1st Underwater Acoustics Conference, Corfu, 24-28 June 2013
- [4] E.K. Skarsoulis, B.D. Cornuelle, M.A. Dzieciuch, Long-range asymptotic behavior of vertical travel-time sensitivity kernels, *Journal of the Acoustical Society of America*, Vol. 134, pp. 3201–3210, 2013.
- [5] M.A. Dzieciuch, B.D. Cornuelle, E.K. Skarsoulis, Structure and stability of wave-theoretic kernels in the ocean, *Journal of the Acoustical Society of America*, Vol. 134, pp. 3318–3331, 2013.
- [6] E.K. Skarsoulis, B.D. Cornuelle, M.A. Dzieciuch, Travel-time sensitivity kernels in a shallow-water environment, in Proc. 2nd Underwater Acoustics Conference, Rhodes, 23-27 June 2014